Flexural Behavior of Glass Fiber Reinforced Silica Composites via Multiple Infiltration Processing

Faizan Siddique Awan (faizanemuhammad38@gmail.com)
Institute of Space Technology https://orcid.org/0000-0003-3985-1040
Raheela Rasheed
Institute of Space Technology
Ibrahim Qazi
Institute of Space Technology
Muhammad Umar Saeed
Institute of Space Technology

Research Article

Keywords: Glass fibers, Silica matrix composites, Silica sol infiltration, Flexural properties, Microstructural characterization

Posted Date: July 15th, 2020

DOI: https://doi.org/10.21203/rs.3.rs-41201/v1

Abstract

Two-dimensional glass fibers reinforced silica matrix composites (GFS) were fabricated by silica sol infiltration (SSI) method by varying the number of infiltration cycles. A uniform weight gain was observed after each infiltration up to 9 th infiltration suggesting the uniform loading of nano silica within GFS composites. The relationship between the infiltration cycle and the physical and flexural behavior of composites was measured by means of a density and 3-point flexural test along with supporting evidences via microstructural characterization. The results of mechanical testing indicated an increase in the flexural properties by up to 25%, after each infiltration cycle, due to increase in density. Finally, microstructural study revealed the presence of various toughening mechanisms during fracture, under flexural loading in the GFS composites.

1 Introduction

Advanced ceramics are an important class of engineering materials which offer numerous enhancements in performance, durability, reliability, hardness, high mechanical strength at high temperature, stiffness, low density,, electrical, and thermal insulation, radiation resistance, and so on. [1, 2]. Among various ceramics materials, silica exhibits a unique combination of properties such as high melting point with high fracture toughness, which makes it suitable for various technological applications [3]. However, direct application of monolithic silica for structural components is not appropriate due to its inferior flexural strength (20–30 MPa), lower compression strength (60 MPa) and extremely low fracture toughness (0.62 MPa m½) [4]. Thus, it is necessary to improve mechanical properties of monolithic silica to make it acceptable for certain structural applications.

One of the means of achieving advanced ceramic materials with improved mechanical properties is by using either particulate or networks of continuous fibers as reinforcements with silica as a matrix material. This leads to newer structural materials, known as fiber-reinforced ceramic–matrix composites [4, 5]. It is expected that a combination of glass fiber as a reinforcement and silica as a matrix has the potential to overcome the drawbacks of brittleness with enhanced damage tolerance.

Literature shows that silica matrix based composites can produce near net shape products with improved fracture toughness and impact resistance at minimal cost than monolithic silica [6]. However, in comparison to particulate based silica composites, continuous silica fiber reinforced silica matrix composites has gained more attention. Such composites can be developed at relatively higher temperatures through chemical vapor infiltration and hot slurry impregnation methods, however the risk of fiber degradation at high temperatures limits the effectiveness and utilization of such methods. In addition, high temperature treatment in oxidizing environments introduces a limitation to thermo-mechanical and thermo-chemical compatibilities [7–9]. On the other hand, a relatively newer processing method to fabricate continuous fiber reinforced silica matrix composites in the form of sol infiltration (SI) technique has emerged as a promising alternative to high temperature processing routes.

The SI method involves low densification temperatures with minimal shrinkage and reduced drying stresses. The utility of SI method as an effective silica matrix composites fabrication technique has been presented in recent studies conducted by numerous researchers [5, 10, 11]. These researchers have incorporated continuous silica fibers with silica matrix through silica sol infiltration (SSI) technique to obtain a silica matrix composite with enhanced mechanical properties [4, 5, 12, 13]. Prasad et al. studied the elastic behavior of silica-silica fiber-reinforced ceramic matrix composites that were fabricated through silica sol infiltration sintering method (SIS) [14]. Similarly, Kim et al. also studied the mechanical properties of 2-D silica-silica continuous fiber reinforced ceramic matrix composites [15]. Also, Liu et al. incorporated 2.5D silica fibers into silica matrix through SIS process to achieve a toughening effect in composites [16]. Additionally, Li et al. prepared 3D seven directional braided silica composites through SIS approach [13]. In another study Liu et al. performed mechanical testing of 2.5D silica reinforced composites prepared through SIS approach. The achieved flexural strength for shallow bend joint was 50.3 MPa while for shallow straight joint the strength was 48.4 MPa [16]. These researchers concluded that the incorporation of continuous silica fibers into silica matrix provided the composites with a kind of pseudo ductility by preventing catastrophic crack growth by such mechanisms as fiber debonding, matrix cracking, fiber-pull out and bridging effect.

In the present study, a systematic yet relatively a fresh approach has been defined to develop glass fibers reinforced silica matrix (GFS) composites through SSI method. This method was selected due to its effectiveness in relatively low densification temperature, low shrinkage and reduced drying stresses. The approach involves multiple infiltrations of silica sol into fabric preform under vacuum followed by multiple drying cycles. The multiple infiltrations, aid in homogenizing the distribution of nano silica in the preform and vacuum assistance ensure maximum voids removal. To study the behavior of GFS composites, microscopic characterization of the fibrous preform was performed after 3rd, 5th, 7th and 9th infiltration cycles. The coating of nano silica on preform after selected infiltration cycles were investigated under a field emission scanning electron microscope. Afterwards, mechanical testing was performed on final sintered GFS composites to assess the strength and flexural behavior of GFS composites. Finally, the results were compared with the available data in terms of relative improvement in mechanical properties.

2 Experimental

2.1 Materials

A 2/2 twill weave E glass fabric was procured from China (Fig. 1a). The average diameter of single fiber was ~ 7 μm. Colloidal silica sol having 30 vol. % SiO_2 content was obtained from Sigma Aldrich (Fig. 1b). The diameter of nano silica was 10–12 nm and purity level was > 90%.

2.2 Manufacturing

2.2.1 Silica Sol Infiltration

Vacuum assisted infiltration process was opted to fabricate GFS composites. Multiple infiltrations were employed to improve the quality of GFS composites. Fourteen layers of 2D woven dry glass fabric were cut into equal dimensions of 200 mm x 200 mm and placed over an aluminum plate to prepare the setup for infusion. Afterwards, a polyester peel ply, a distribution mesh and resin in-out pipes were attached and adjusted accordingly. An airtight nylon vacuum bag was placed over the setup and a vacuum pump was attached to generate a constant vacuum pressure of 0.9 bar for 01 hour. The infiltration of sol was kept at a slow rate in order to achieve complete wetting of fibrous preform. Subsequently, the pump was switched off while keeping the setup under vacuum.

2.2.2 Drying Cycle

The wet preform setup was then placed in an oven at 80 °C for 1 hour followed by drying at 110 °C for another hour as shown in Fig. 2. This heating removed the coupling agent and bound water present in the sol. The same drying process was repeated after each infiltration cycle.

2.2.3 Sintering of composites

Finally, the GFS composite panel was sintered at 550 °C for 2 hours. The samples of required dimensions were cut from the composite panels for microstructural and mechanical property characterization.

2.3 Testing and Characterization

The densities of sintered composites were measured using a densimeter (AU-900S, Dong Guan Hong Tuo Instrument Company, Guangdong, China) with an accuracy of 10^{-3} g.

The flexural strength and flexural behavior of the composites were determined by a three-point bend test following ASTM standard C1341 [17]. The test was performed on a universal testing machine (WDW-30, Jinan Testing Equipment IE Corporation, Jinan, China). The strain rate used for the testing of specimens of dimensions 35 × 5 × 3.5 mm was 0.1 mm/min, while at least five tests of each composite were performed. The samples were cut using a low speed cutter (Buehler Isomet, ITW Company, Lake Bluff, Illinois).

Scanning Electron Microscopy (SEM) of the composites was performed on a field emission microscope (MIRA-III, FEG-SEM, Tescan Orsay Holding, Brno, Czech Republic). Images were acquired in the secondary electron mode at an operating voltage of 5 kV. The samples were placed on an aluminum stub with carbon tape. The fracture surfaces of GFS composite specimens were also studied via SEM to investigate the fracture morphology.

3 Results And Discussions

3.1 Weight Gain

The weight of GFS composite was measured before and after infiltration as shown in Fig. 3. With each infiltration the weight gain increased, however after the 7th infiltration a steady weight gain was observed. The initial increase in weight gain could be attributed to voids and open spaces that were filled with silica sol. The relative change in weight gain decreased with successive infiltration cycles, apparent from the slope (tangent) of the curves in Fig. 3. However, the weight gain reached a maximum at the 9th infiltration cycle.

3.2 Density

Figure 4 shows the variation of density vs. number of infiltration cycles. The density shows an increasing trend. The reason for the initially low density is the presence of voids due to absence of enough silica and lower compaction of the GFS composites. However, with increase in infiltration cycles, the voids or empty spaces get filled with silica matrix, resulting in a more compact composite structure with enhanced density. As evident from Fig. 4 (a-d) the density after the 3rd cycle increased from 1.56 g/cm^3 to 1.84 g/cm^3 after the 9th infiltration cycle. This trend in increase in density is similar to previously reported work of Han et al [18] & Liu et al [4, 16]. After the silica reaches saturation; there is hardly any change in the density, with further infiltration cycles. The highest density achieved in this research work was 1.84 g/cm^3 after the 9th infiltration cycles which is about 4% higher than previously reported by Liu et al [4, 16].

3.3 Microscopy of silica coated glass fibers

SEM was performed to observe the extent of silica deposition on GFs as shown in Fig. 5. The gradual increase in silica content can be observed. Figure 5 (a) confirms the presence of silica as matrix around bare fibers. Similarly, Fig. 5 (b) and (c) shows (at higher magnification) the presence of brittle matrix around stiff fibers. Figures 5 (d-f) shows increase in matrix, with the gap between fiber and the matrix being a manifestation of the weak interfacial bonding. However, Figs. 5 (g-i) depicts the increase in silica quantity as the pores are increasingly filled. The gap between fiber and matrix has reduced with matrix covering more than half of the fibers. Accordingly, it can also be seen from Figs. 5 (j-k) an almost complete coverage of fibers with the silica matrix. Surface roughness has also increased indicating enhanced interfacial bonding between fibers and the matrix. The matrix around fibers shows absence of gaps.

3.4 Flexural Strength

The flexural properties of GFS composites are shown in Fig. 6. All the samples were tested under same conditions by keeping the fiber volume constant. The change in properties was studied as function of silica content (infiltration cycles). It is evident that with increasing silica content, the overall flexural properties of GFS composite improves. The flexural strength of GFS-3 composite (after three infiltration cycles) was found to be 18.96 ± 0.01 MPa which is significantly low due to high levels of porosity. Whereas from GFS-5 onwards, the silica matrix showed strengthening effect. The average flexural

strength of the composite after five infiltrations was 24 ± 0.02 MPa which was 20% more than the value of GFS-3 composite. Similarly, GFS-7 composite showed an improvement of 18% with an average strength of 28.18 ± 0.025 MPa. Finally, after nine infiltration cycles, GFS-9 composite showed an improvement of 27% as compared to GFS-7 composite with an average value of 39.10 ± 0.03 MPa. In a comparable study on the mechanical behavior of 2D woven silica fibers reinforced ceramics matrix composites, Kim et al. has reported a maximum flexural strength of 23.2 MPa after 09 infiltration cycles [15].

3.5 Flexural Behavior

Figure 7 shows the stress-strain curves for GFS-5 to GFS-9 composites. The graphs indicate that initially matrix cracking occurs in the composite as represented by point “a” in each curve, followed by F/M debonding shown as point “b” and then the failure induced by fiber pull-out and/or crack deflection mechanisms shown as point “c”. The composites exhibits time delayed fracture producing strain via fiber pull-out. The areas under the stress-strain graph is indicative of the amount of energy absorbed by the composite during failure and the fracture toughness could be estimated via the area size [19]. However, the variation in the degree of nonlinearity and strain values might cause disparity in toughness values of these composites, as previously reported by Liu et al [20].

The data in Fig. 7 (a-c) reveals that with successive increasing infiltration, the strain decreased and strength increased. The silica concentration influenced the fiber-matrix (F/M) interfacial bonding and hence the behavior of the GFS composites. Similar behavior has been reported previously [21]. With successive infiltrations, the pores among glass fibers were filled with silica matrix; that established a strong F/M bonding which hindered crack propagation. In case of GFS-5 (Fig. 7-a) the F/M interface bonding is relatively weak, the crack deflects at various planes instead of penetrating through the fibers causing fiber pullout. In case of GFS-7 (Fig. 7-b) the fiber pullout is low, fracture therefore occurs at low strain. A similar behavior was observed and reported by Li et al. [16] and Dassios et al. [22] in their studies on continuous fiber reinforced silica matrix composites. In GFS-9 (Fig. 7-c), the matrix concentration being much higher than the previous cycles, the matrix cracks at a high stress and low strain. The low strain indicates that F/M debonding was difficult, therefore fracture occurs sooner in comparison to previous cycles.

3.6 Fractography

Fractured surfaces of failed samples are shown in Fig. 8. The feature in the micrographs supports the failure mechanism proposed in the previous section. The failure is a combination of matrix cracking, F/M debonding, crack deflection and fiber pullout. The elongation in GFS composites mainly depends on deflection of the crack at F/M interface and the magnitude of pullout length. With successive infiltration cycles the fracture toughness of GFS composite decreased although the strength increased, consistent with the study reported by Liu et al [20]

The GFS-3 fractograph as shown in Fig. 8-a manifests a multistep broom like failure with extensive fiber pullout; an indication of weak F/M interface where debonding was relatively easy due to low matrix concentration and compaction. The GFS-5 fractograph in Fig. 8 (b) exhibits a large amount of matrix along the fibers indicating the adherence of the matrix to the fibers, making that F/M interface bonding relatively stronger than GFS-3 composite. Similarly, the GFS-7 fractograph as shown in Fig. 8 (c) depicts multiple crack deflection with minimal fiber pullout as compared to GFS-5 composite. Finally, the GFS-9 in Fig. 8 (d) illustrates the fiber fracture at various planes with almost negligible magnitude of fiber pullout. Additionally, the fiber surface was ragged, indicative of fiber cracking along a cleavage plane. The fiber failure rather than pullout indicates that failure is occurring in the same plane, simultaneously in the matrix and the fiber. All GFS composites fractured in translaminar fashion. Because the fracture strain of fiber is higher, therefore when load was increased, the composite deformed elastically with small strain, until micro cracks developed, and coalesced in the brittle matrix.

- **Conclusions**

Glass fiber reinforced silica (GFS) composites were successfully developed through vacuum assisted silica sol infiltration (SSI) technique. The matrix was silica sol while the reinforcing material was glass fiber. The study shows that variation in matrix concentration has a strong influence on the physical and mechanical properties of GFS composites. As the porosity decreased, the density of the GFS composites increased from ~ 1.54 g/cm^3 to ~ 1.84 g/cm^3. The flexural strength increased to ~ 40 ± 0.01 MPa in GFS-9 from 18.91 ± 0.02 in GFS-3, exhibiting an overwhelming increase of about 50% in the flexural strength along with a quasi-ductile behavior under loading.

References

1. Li L (2016) Fatigue life prediction of fiber-reinforced ceramic-matrix composites with different fiber preforms at room and elevated temperatures. Mater 9:207
2. Rosso M, Ceramic and metal matrix composites: route and properties 12th international scientific conference achievements in mechanical and materials engineeringPolytechnic of Turin, Dep. of Material Science and Chemical Engineering, C.so Duca degli Abruzzi, 24 10129 Torino, Italy 2003
3. LIU Y, CHEN Z, ZHU J, MECHANICAL PROPERTIES AND CHARACTERIZATION OF A NOVEL COUPLED 2.5 D BRAIDED SiO2f/SiO2 COMPOSITE, 15TH EUROPEAN CONFERENCE ON COMPOSITE MATERIALSItaly, 2012
4. Liu Y, Zhu J, Chen Z, Jiang Y, Li B, Chen Z, Lin L, Guan T, Li C (2012) Mechanical properties and microstructure of 2.5 D (shallow bend-joint) quartzf/silica composites by silicasol-infiltration-sintering. SCI ENG COMPOS MATER 19:55–59
5. Liu Y, Zhu J, Chen Z, Jiang Y, Li B, Lin L, Guan T, Cong X, Li C (2012) Mechanical behavior of 2.5 D (shallow bend-joint) and 3D orthogonal quartzf/silica composites by silicasol-infiltration-sintering. Mater Sci Eng A 532:230–235

6. Pamuk G, Çeken F (2008) Manufacturing of weft-knitted fabric reinforced composite materials: a review. MATER MANUF PROCESS 23:635–640
7. Qi G, Zhang C, Hu H (2007) High strength three-dimensional silica fiber reinforced silicon nitride-based composites via polyhydridomethylsilazane pyrolysis. Ceram Int 33:891–894
8. Naslain RR (1998) The design of the fibre-matrix interfacial zone in ceramic matrix composites. Compos Part A Appl Sci 29:1145–1155
9. Li C, Chen Z, Zhu J, Liu Y, Jiang Y, Guan T, Li B, Lin L (2012) Mechanical properties and microstructure of 3D orthogonal quartz fiber reinforced silica composites fabricated by silicasol-infiltration-sintering. Materials Design 36:289–295 (1980–2015)
10. Liu Y, Zhu J, Chen Z, Mechanical Properties of Two Kinds of 2.5 D Quartz f/Silica Composites by Silica Sol-Infiltration-Sintering, Asian J. Chem., 25 (2013)
11. Ko S-Y, Yong S-M, Lee S, Cheong D-I, Baek S, Effect of Additives on the Densification Processes and Properties of Silica-Based CMCs, Archives of Metallurgy and Materials, 63 (2018)
12. Liu H-K, Huang C-C (2001) Impact response and mechanical behavior of 3-D ceramic matrix composites. J Eur Ceram 21:251–261
13. Li B, Zhu J, Jiang Y, Lin L, Liu Y, Chen Z (2012) Processing and flexural properties of 3D, seven-directional braided (SiO2) f/SiO2 composites prepared by silica sol-infiltration-sintering method. Ceram Int 38:2209–2212
14. Prasad NE, Loidl D, Vijayakumar M, Kromp K (2004) Elastic properties of silica–silica continuous fibre-reinforced, ceramic matrix composites. Scr Mater 50:1121–1126
15. Kim H-N, Kim D-J, Kang E-S, Kim D-K (2009) Mechanical Properties of 2-D Silica-Silica Continuous Fiber-reinforced Ceramic-matrix Composite Fabricated by Sol-Gel Infiltration. Korean J Mater Res 19:391–396
16. Liu Y, Zhu J, Chen Z, Jiang Y, Li C, Li B, Lin L, Guan T, Chen Z (2012) Mechanical properties and microstructure of 2.5 D (shallow straight-joint) quartz fibers-reinforced silica composites by silicasol-infiltration-sintering. Ceram Int 38:795–800
17. Yonathan P, Lee J-H, Yoon D-H, Kim W-J, Park J-Y (2009) Improvement of SiCf/SiC density by slurry infiltration and tape stacking. Mater Res Bull 44:2116–2122
18. Han SA, Jiang KH, Tang JW, Studies on preparation and property of 2.5 D SiO2f/SiO2 composites, Advanced Materials Research, Trans Tech Publ, 2009, pp. 1767–1770
19. Liu Y, Zhu J, Chen Z, Jiang Y (2012) Mechanical behavior of 2.5 D (shallow straight-joint) and 3D four-directional braided SiO2f/SiO2 composites. Ceram Int 38:4245–4251
20. Liu Y, Chen Z, Zhu J, Jiang Y, Li B, Boafo FE (2012) Comparison of 3D four-directional and five-directional braided SiO2f/SiO2 composites with respect to mechanical properties and fracture behavior. Mater Sci Eng A 558:170–174
21. Carrère N, Martin E, Lamon J (2000) The influence of the interphase and associated interfaces on the deflection of matrix cracks in ceramic matrix composites. Compos Part A: Appl Sci Manufac

31:1179–1190

22. Dassios KG, Galiotis C, Kostopoulos V, Steen M (2003) Direct in situ measurements of bridging stresses in CFCCs. Acta Mater 51:5359–5373

Figures

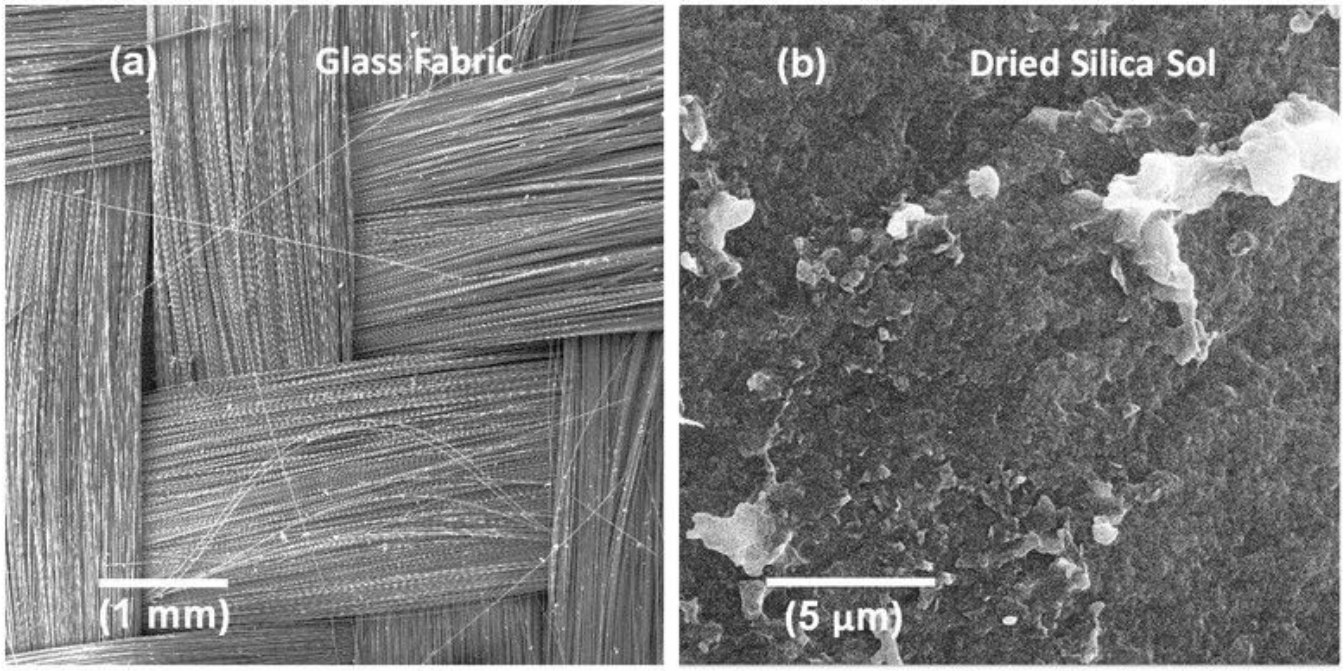

Figure 1

Materials used in GFS composite development: (a) Glass fabric (b) Dried silica sol

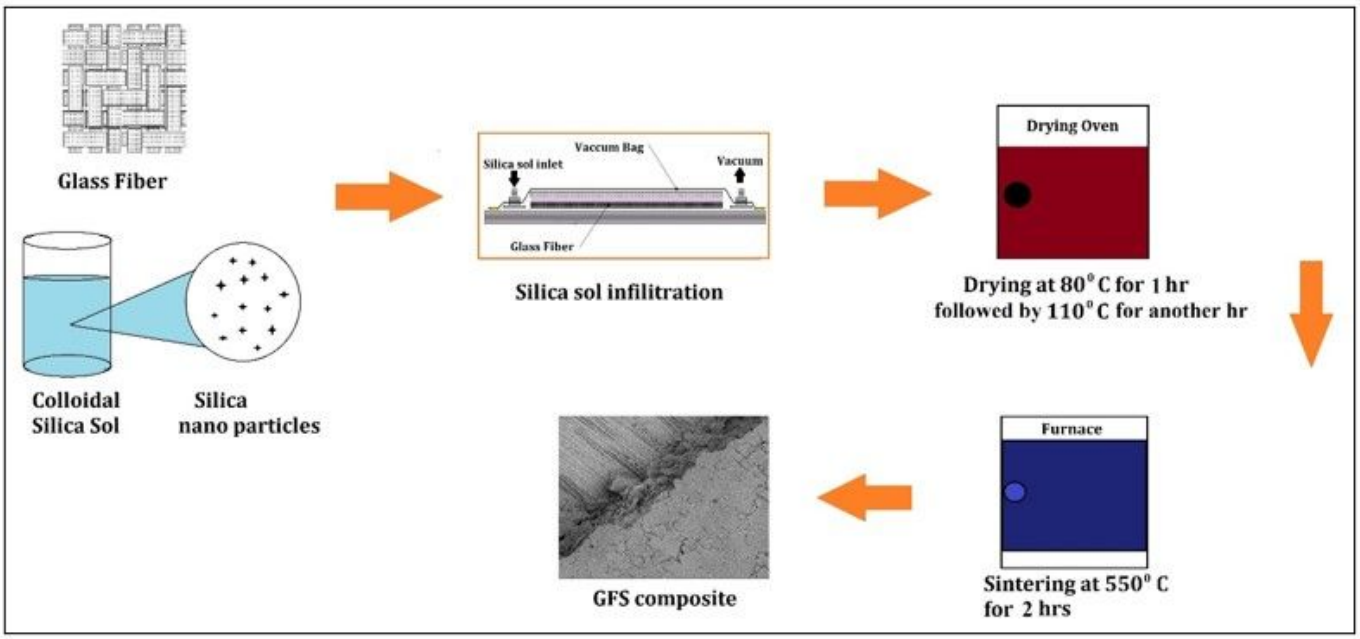

Figure 2

Schematic diagram showing steps involved in GFS composite development

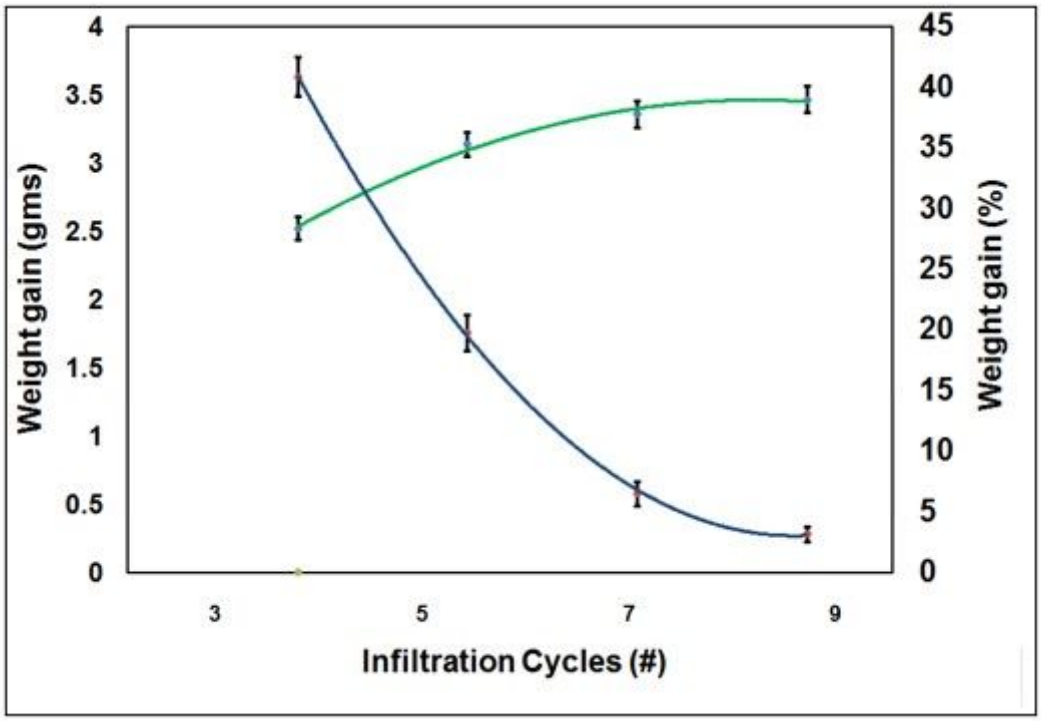

Figure 3

Weight gain and percentage weight gain after each infiltration

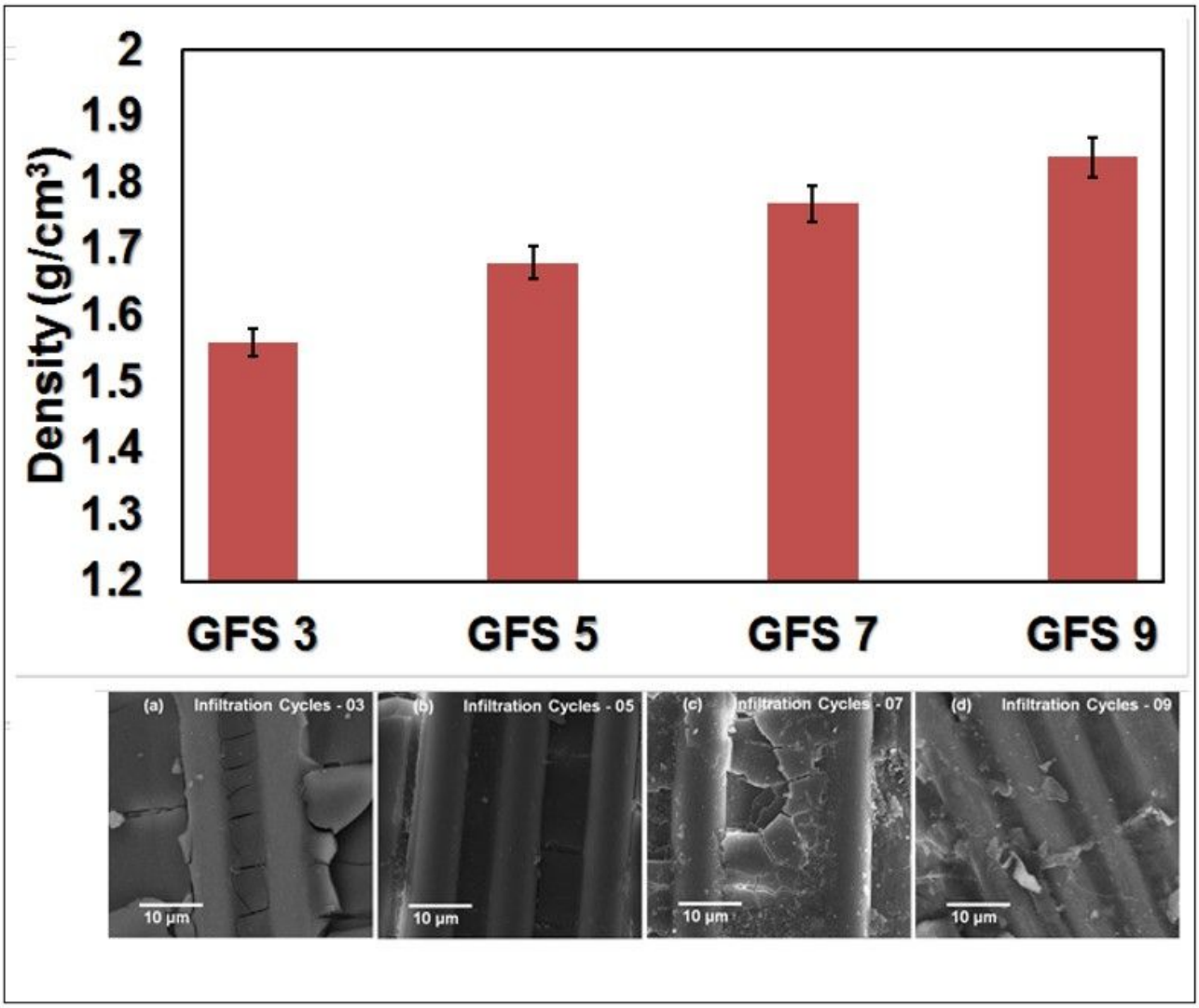

Figure 4

SEM micrographs of GFS composites showing increase in silica content after multiple infiltrations

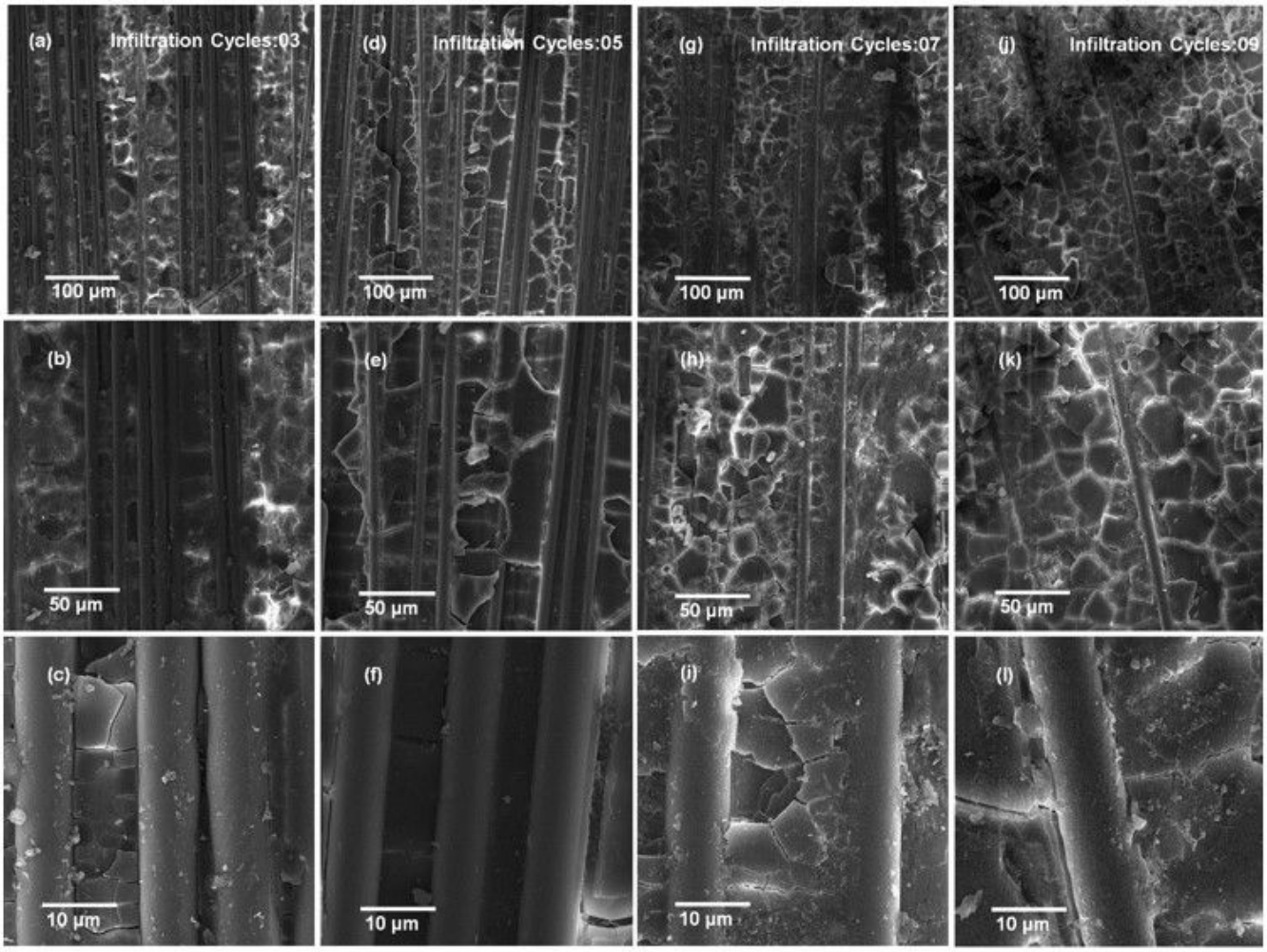

Figure 5

SEM micrographs of GFS composites: (a-c) GFS -3, (d-f) GFS -5, (g-i) GFS -7 and (j-l) GFS -9

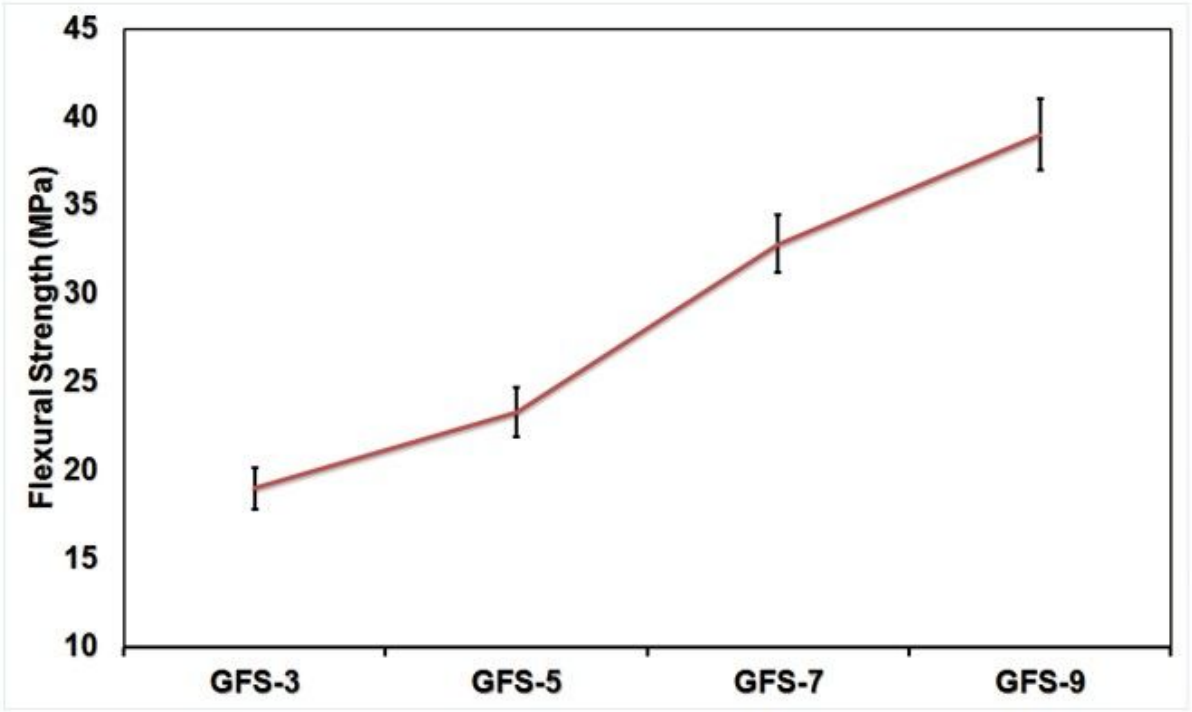

Figure 6

Flexural strength of GFS composite after each infiltration

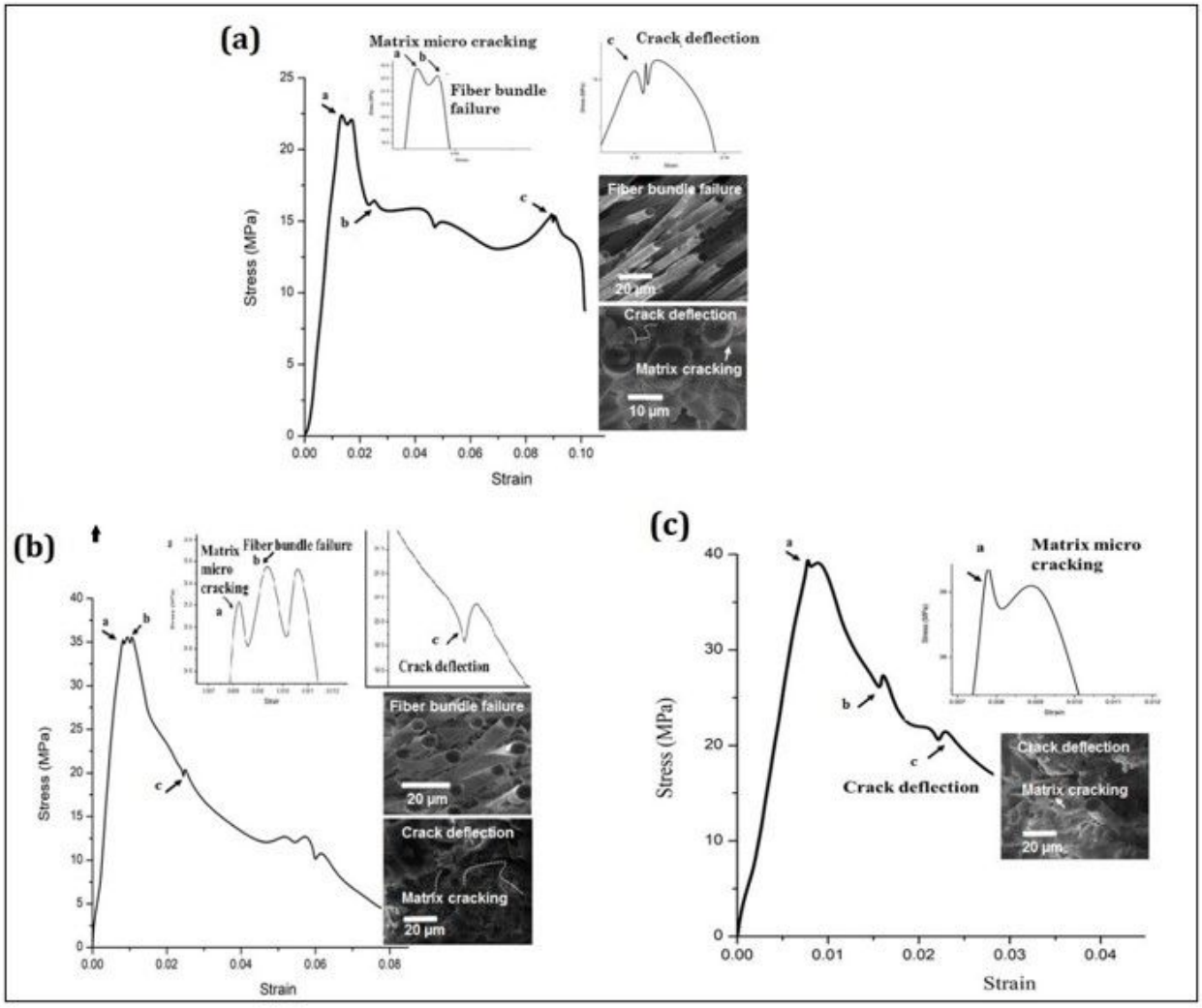

Figure 7

Flexural properties of GFS composites: (a) stress-strain curve of GFS -5, (b) stress-strain curve of GFS -7 and (c) stress-strain curve of GFS -9

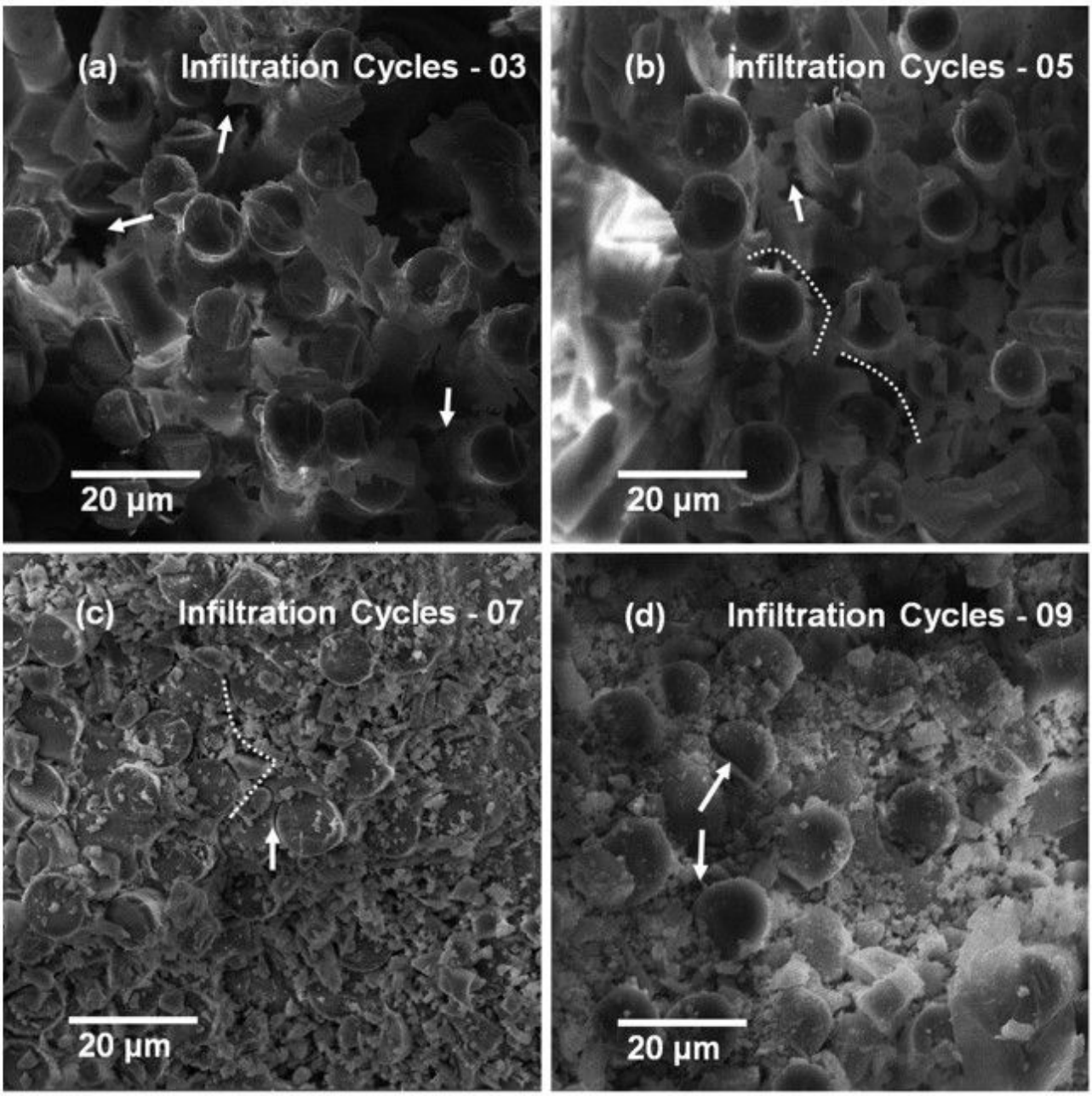

Figure 8

SEM micrographs of fracture surfaces: (a) GFS - 3, (b) GFS - 5, (c) GFS - 7 and (d) GFS - 9

Supplementary Files

This is a list of supplementary files associated with this preprint. Click to download.

- GAbstract.jpg
- GAbstract.jpg